Depth dependence of the ionization energy of shallow hydrogen states in ZnO and CdS

T. Prokscha,[1,*] H. Luetkens,[1] E. Morenzoni,[1] G. J. Nieuwenhuys,[1,2,†] A. Suter,[1] M. Döbeli,[3] M. Horisberger,[4] and E. Pomjakushina[4]

[1]*Laboratory for Muon Spin Spectroscopy, Paul Scherrer Institut, CH-5232 Villigen PSI, Switzerland*
[2]*Kamerlingh Onnes Laboratory, Leiden University, 2300 RA Leiden, The Netherlands*
[3]*Ion Beam Physics, ETH Zurich, CH-8093 Zurich, Switzerland*
[4]*Laboratory for Developments and Methods, Paul Scherrer Institut, CH-5232 Villigen PSI, Switzerland*

(Received 29 August 2014; revised manuscript received 18 November 2014; published 1 December 2014)

The characteristics of shallow hydrogenlike muonium (Mu) states in nominally undoped ZnO and CdS (0001) crystals have been studied close to the surface at depths in the range of 10–180 nm by using low-energy muons and in the bulk using conventional μSR. The muon implantation depths are adjusted by tuning the energy of the low-energy muons between 2.5 and 30 keV. We find that the bulk ionization energy E_i of the shallow donorlike Mu state is lowered by about 10 meV at a depth of 100 nm, and continuously decreasing on approaching the surface. At a depth of about 10 nm, E_i is further reduced by 25–30 meV compared to its bulk value. We attribute this change to the presence of electric fields due to band bending close to the surface, and we determine the depth profile of the electric field within a simple one-dimensional model.

DOI: 10.1103/PhysRevB.90.235303 PACS number(s): 71.55.Gs, 73.40.Vz, 61.72.uj, 76.75.+i

I. INTRODUCTION

For future semiconductor technologies, the incorporation, profiling, and monitoring of dopants are considered to be key issues for novel device applications [1]. The binding energy of a dopant is an important characteristic, and recent studies have focused on the investigation of the binding energies of single hydrogenic defect states close to semiconductor surfaces, in nanoscale devices, or in quantum wells [2–5]. For a shallow Coulombic hydrogenic impurity state in the effective mass approximation, the binding energy of the state is predicted to decrease when approaching a potential barrier at a semiconductor interface or surface [6,7]. A model proposed by Levine [8] showed that at a semiconductor surface the ground state of a shallow impurity is the $2p$ state, which means that the binding energy of the surface donor is 1/4 of the bulk donor. However, image charges at the surface cause the binding energy to be closer to its bulk value, while still being reduced [9]. In contrast, recent theoretical studies found an *increase* of the hydrogenic impurity binding energies in nanowires and quantum dots due to dielectric confinement [10,11]. Additionally, an experimental investigation of Si doped GaAs estimated an increasing binding energy at depths $z < 1.5$ nm [5], and the authors concluded that the effective mass approach will fail for all hydrogenic donors close to a semiconductor surface.

The descibed effects so far occur on a length scale of typically less than ten nanometers. In this paper, we will discuss the change of the binding energy of single shallow hydrogenlike donor states on a much larger length scale at depths between 10 nm and ∼200 nm, where the effective mass approximation appears to be appropriate, and dielectric confinement and position dependent effective masses or dielectric constants are negligible. Even in the case of band bending at the surface—which is of particular importance for this work—the effective mass approximation is expected to hold because the fractional change of the perturbation potential over the dimension of a unit cell is negligibly small [12,13] (less than 1% in our case). In case of good sample quality with dislocation line densities $\lesssim 10^5$ cm^{-2}, the effect of internal strain, due to these dislocations, on the ionization energy of shallow donor states can be neglected [14]. However, the donor ionization energy may be affected by the presence of electric fields close to the sample surface: in a lowly doped semiconductor, surface states can cause a pinning of the Fermi level at the surface, which results in a band bending on a length scale given by the Debye length [15]. In this case, the solution of the Poisson equation yields an quadratic z dependence of the electrostatic potential in the band bending zone close to the surface [15], which means a linearly increasing electric field towards the surface. The presence of an electric field lowers the ionization energy of the shallow impurity (Poole-Frenkel effect in insulators or semiconductors [15–18]), and since the electric field increases on approaching the surface, the binding energy is expected to decrease when getting closer to the surface.

Hydrogen as an ubiquitous impurity is of particular interest in semiconductor technology, because it often modifies the electrical and optical properties in an unwanted way due to its amphoteric behavior, which may cause doping counteracting the prevailing type of conductivity. The characterization of hydrogen impurities in semiconductors is often difficult, particularly if one wants to study single (or solitary) dopants. Here, positively charged muons (μ^+) can help to circumvent these difficulties. Muons played an important role in the identification and characterization of isolated hydrogen defect centers in semiconductors [19–22]. Implanted in a semiconductor or insulator the μ^+ stops at an interstitial site, and may capture one or two electrons to form the light hydrogen pseudoisotope muonium [Mu, (μ^+e^-), mass of $\mu^+ \simeq 1/9$ proton masses]. Depending on the concentration of other dopants, and on Mu formation energy, it occurs in either of three charge states Mu$^+$, Mu^0, or Mu$^-$, analogous to hydrogen. The neutral state can be spectroscopically distinguished from the charged states in muon spin rotation experiments (μSR)

*thomas.prokscha@psi.ch
†Deceased.

 ©2014 American Physical Society

[23]. The recent theoretical discovery of a universal alignment of the so-called hydrogen pinning level $\varepsilon(+/-)$—where the formation energies of the positive and negative impurity are equal—allows predictions whether hydrogen forms a shallow donor: this occurs if the pinning level is close to or above the conduction band minimum [24,25]. The predicted shallow hydrogen donor states in ZnO [26] and InN [25] have been first confirmed by μSR measurements [27,28], closely followed in ZnO by EPR [29] and infrared spectroscopy [30,31]. In CdS, the observed shallow Mu state [32,33] does not necessarily imply, according to the theoretical models, that in thermodynamic equilibrium hydrogen acts as a shallow donor. Since the muon experiments take place on a microsecond time scale (muon life time is $\sim$2.2 μs), the observed shallow Mu state could be a metastable state [34–36].

In this paper, we present the depth dependence of the ionization energy of the shallow Mu state in CdS and of the shallow donor state in ZnO, and at the interface of a 20-nm-thin Au film sputtered on ZnO. This allows us to obtain direct information about the effect of electric fields—due to band bending—on the ionization energies of the corresponding hydrogenlike states in a range of $\sim$200 nm beneath the surface, or at a metal-semiconductor interface. The ionization energies continuously decrease on approaching the surface/interface, reaching a reduction of 25–30 meV at a depth of 10 nm. We use the observed "ionization profile" to determine by a simple one-dimensional model the electric field profile at the surface/interface. This is to best of our knowledge the first time that the "ionization profile" of a single impurity and the derived electric field profile has been visualized by means of a *local probe* implantation technique. It offers several advantages compared to conventional experimental techniques. Photoemission spectroscopy and other surface sensitive techniques (see the review of Koenraad and Flatté [1] and references therein) are limited to a few surface layers, and cannot access interfaces at a depth of tens of nanometers. Deep-level transient spectroscopy is not applicable to low-doped materials, shallow impurity states, and single dopants, and usually requires a *p-n* junction. In contrast, there are no such limitations for muon spin rotation, which is contactless, and provides intrinsic information, about shallow as well as deep hydrogen states. They are incorporated as solitary dopants, and their properties can be monitored as a function of distance to the surface or an interface, thus providing a new experimental tool to address the issues raised at the beginning of this introduction.

II. EXPERIMENTAL DETAILS

The μSR experiments were carried out at the Swiss Muon Source (SμS, Paul Scherrer Institut, Villigen, Switzerland). For the near-surface measurements at mean depths $\langle z\rangle <$ 200 nm, we used the low-energy μSR spectrometer (LE-μSR) LEM at the μE4 beam line [39,40]. Polarized low-energy μ^+ with energies in the keV range are generated by moderation of a 4-MeV muon beam in a solid, about 250-nm-thin Ar film with a $\sim$10-nm-thin N_2 capping layer, deposited at 10 K on a patterned Ag foil [41–44]. Epithermal muons with a mean energy of $\sim$15 eV escape into vacuum with a conversion efficiency from MeV-to-eV of $\sim 5\times10^{-5}$. They

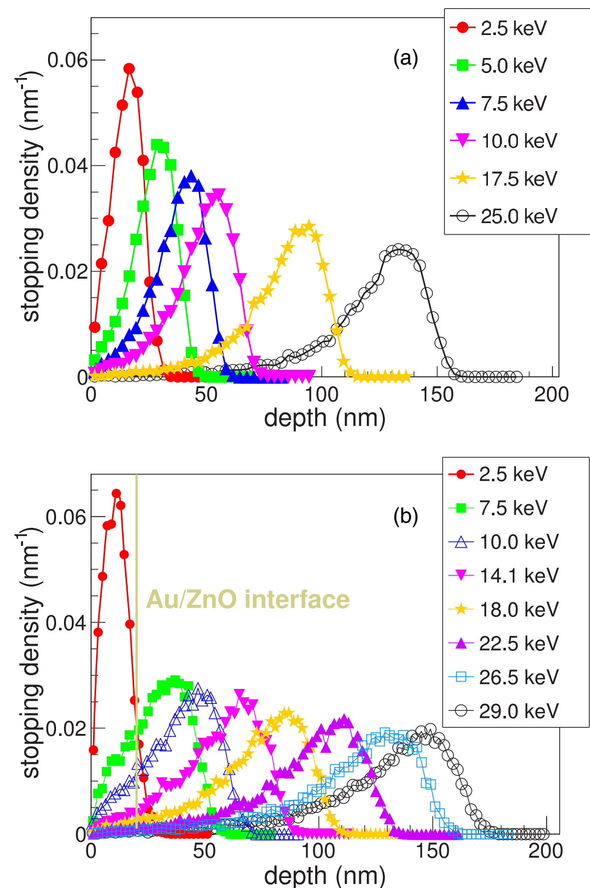

FIG. 1. (Color online) Simulated muon implantation profiles in (a) ZnO and (b) 20-nm Au on top of ZnO, using the program TRIMSP [37], which has been shown to calculate the stopping profile with sufficient accuracy [38].

are accelerated electrostatically to energies up to 20 keV by applying a positive bias to the Ag moderator foil, and then transported by use of electrostatic elements over a distance of about two meters to the sample cryostat. The muon implantation energy was varied between 2.5 and 30 keV, corresponding to mean implantation depths of 10 and 150 nm, respectively, see Fig. 1. The implantation energy is usually varied by applying a positive or negative bias of up to 12 kV to the electrically insulated sample holder [39]. Shallow Mu formation deep in the bulk at $\langle z\rangle \sim$ 200–300 μm was studied at the GPS spectrometer at the πM3 beam line with a muon beam energy of about 3.5 MeV.

The samples were nominally undoped ZnO and CdS wafers [(0001) orientation, supplier: Crystec GmbH, Berlin, Germany; resistivity >10 Ωcm and >1 kΩcm, respectively]. The ZnO crystals had a size of 10 × 10 mm^2 and a thickness of 0.5 mm. Nine pieces were glued with conductive silver onto a standard sample plate of LEM. This mosaic of samples ensured that no muons missed the sample, therefore eliminating any background contribution (the low-energy muon beam spot has a FWHM of about 13 mm). In the second experiment, several pieces of the ZnO crystals were sputtered with a 20-nm-thin Au film to study any changes introduced by the Schottky barrier at the Au/ZnO interface. The CdS sample was one half of a 2" wafer, 0.5-mm thick, which was also large enough to stop all

muons in the sample. All samples were polished on both sides. For the GPS measurements, one of the ZnO crystals was used, and a $\sim 5 \times 10$ mm^2 broken-off piece of the CdS wafer.

Transverse field μSR measurements have been performed with a magnetic field of 10-mT applied parallel to the $\langle 0001\rangle$ direction, and the muon spin initially parallel to the sample surface at LEM, and out of plane at GPS. Shallow Mu in CdS and ZnO has an anistropic, axially symmetric hyperfine interaction with the hyperfine coupling constants $A_{\parallel}$ and $A_{\perp}$ parallel and perpendicular to the symmetry axis, which is along the Cd-S or the Zn-O bond direction [32,33]. In the high-field limit, two shallow Mu lines can be observed with a separation $\Delta\nu(\Theta) = A_{\parallel}\cos^2\Theta + A_{\perp}\sin^2\Theta$, where Θ is the angle between the Mu symmetry axis and the externally applied field. The two lines are placed symmetrically around the "central" line, i.e., the precession frequency of bare μ^+ without bound electron. In the geometry of the experiment, there is one shallow Mu state at a bond parallel to the $\langle 0001\rangle$ direction ($\Theta = 0$), and three Mu states at the bonds under $\Theta = 109.4^\circ$ with respect to the $\langle 0001\rangle$ axis. This leads to two pairs of Mu lines with an intensity ratio of 1:3. For ZnO and CdS, the hyperfine couplings are $A_{\parallel} = 760(30)$ and 335(8) kHz, $A_{\perp} = 370(22)$ and 199(6) kHz, respectively [33]. However, only in CdS, the Mu lines are narrow and well resolved in bulk μSR experiments whereas in ZnO, spin and/or charge exchange with impurities or free charge carriers even at low temperatures (5 K) lead to a sizable broadening of the Mu lines, which smears out the Mu satellite lines [32,33]. In CdS, the spitting of the inner lines ($\Theta = 109.4^\circ$) is $\Delta\nu_{\mathrm{I}} = 0.214(5)$ MHz, and the splitting of the outer lines ($\Theta = 0^\circ$) is $\nu_{\mathrm{O}} = 0.335(8)$ MHz. In ZnO, the correponding separations are $\Delta\nu_{\mathrm{I}} = 0.413(20)$ MHz, and $\Delta\nu_{\mathrm{O}} = 0.760(30)$ MHz.

The ratio of ionized to neutral impurities (donors) as a function of temperature T is given by [45]

$$\frac{N_D^+}{N_D^0} = \frac{N_c}{n}\frac{1}{g_D}\exp(-E_i/k_BT) \equiv N\exp(-E_i/k_BT), \quad (1)$$

where N_c is the effective density of states in the conduction band, n is the concentration of free carriers, g_D is the impurity spin degeneracy, E_i is the ionization energy of the donor, and N is a density-of-states parameter. We can rewrite in terms of ionized (f) and unionized $(1-f)$ muonium fractions [46]: $f/(1-f) = N_D^+/N_D^0$. With this it follows for the neutral Mu^0 fraction $f_{\mathrm{Mu}}(T)$:

$$f_{\mathrm{Mu}}(T) = [1 - f(T)] = \frac{1}{1 + N\exp(-E_i/k_BT)}. \quad (2)$$

Thus, by measuring the neutral Mu fraction $f_{\mathrm{Mu}}(T)$ as a function of temperature, the donor ionization energy E_i can be determined. In case of well resolved satellite lines, the μSR asymmetry spectra can be fit by a sum of five Lorentzians (i.e., exponential relaxation in time domain), with the sum A_{Mu} of asymmetries (amplitudes) of the four Mu satellite lines, and the asymmetry A_{D} of the so-called diamagnetic signal, i.e., a μ^+ without bound electron. The neutral fraction $f_{\mathrm{Mu}}(T)$ is then given by

$$f_{\mathrm{Mu}}(T) = \frac{A_{\mathrm{Mu}}(T)}{A_{\mathrm{Mu}}(T) + A_{\mathrm{D}}(T)}. \quad (3)$$

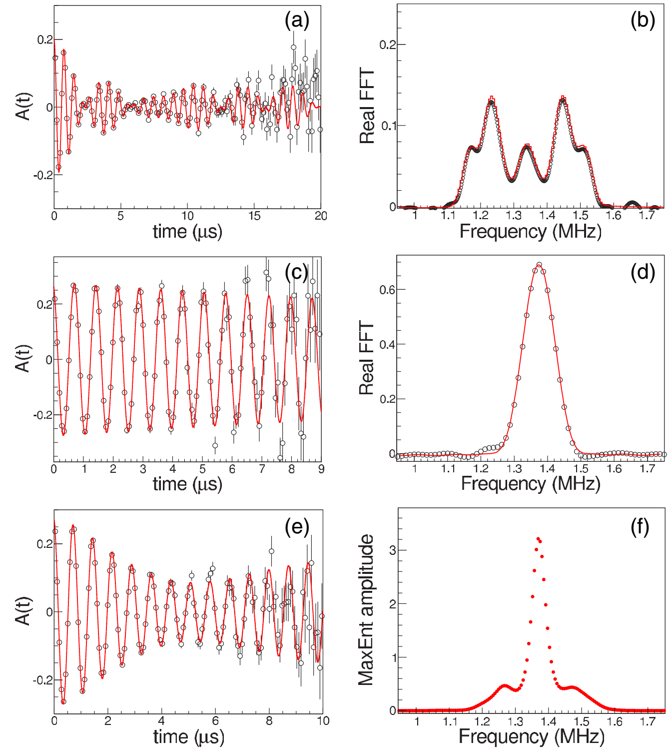

FIG. 2. (Color online) CdS (0001), 10-mT applied parallel to a $\langle 0001\rangle$ direction, μSR asymmetry spectra $A(t)$, and corresponding real part of fast Fourier transform (Real FFT). (a) and (b) 5 K, bulk μSR (GPS instrument, Muons-On-REquest (MORE) mode [50]) ($\langle z\rangle \sim 280$ μm). (c) and (d) 5 K, implantation energy 25 keV, virgin polished sample ($\langle z\rangle \sim 140$ nm). (e) and (f) 5 K, implantation energy 23–26.5 keV, etched sample. The spectrum in (f) is obtained by a maximum entropy fit [51,52] to the data in four positron counters. The solid red lines are fits to the data as described in the text, using the program MUSRFIT [53].

III. RESULTS

Asymmetry and corresponding frequency spectra for CdS and ZnO are shown in Figs. 2 and 4, respectively. The analysis has been done in the following way. In practice, it is difficult to derive the temperature dependence of the neutral fraction by trying to fit five lines to the experimental data over the whole temperature range. Problems arise in this procedure in the case of poorly resolved satellites or small Mu fractions. Also, with increasing temperature spin-exchange processes due to thermally activated charge carriers lead to broadening of the Mu satellites and a phase shift of the Mu signal with respect to the μ^+ signal [47,48]. This makes fits in the ionization regime more difficult: whereas at temperatures $T \lesssim 15$ K the CdS and ZnO data could be fit with five lines, where we fixed the splitting of the Mu lines to the known values, this procedure didn't work well in the ionization regime. Therefore we simplified the analysis by an approximation: in CdS the μSR asymmetry spectra $A(t)$ were fit over the whole temperature range by the sum of two exponentially decaying components:

$$A(t) = [A_{\mathrm{D}}\exp(-\lambda_{\mathrm{D}}t) + A_{\mathrm{Mu}}\exp(-\lambda_{\mathrm{Mu}}t)]\cos(\omega t + \phi), \quad (4)$$

where λ_D is the relaxation rate of the central, diamagnetic line which we fixed to the high temperature value (where Mu is ionized, $\lambda_D \lesssim 0.01\ \mu s^{-1}$), $\omega = \gamma_\mu B$ is the μ^+ precession frequency in the applied magnetic field $B = 10$ mT, and $\gamma_\mu/2\pi = 135.5$ MHz/T is the gyromagnetic ratio of the muon, and ϕ is a detectors phase of the corresponding decay positron detector. In this way, the temperature dependent Mu fraction $f_{Mu}(T)$ can be calculated according to Eq. (3), which is then used to determine the ionization energy by fitting Eq. (2) to $f_{Mu}(T)$. In the case of ZnO and Au/ZnO with poorly resolved satellites, we further simplified the analysis by using a single exponentially relaxing component:

$$A(t) = A \exp(-\lambda t)\cos(\omega t + \phi). \tag{5}$$

The temperature dependence of $\lambda(T)$ can be well approximated by Eq. (2) [49]:

$$\begin{aligned}\lambda(T) &= f_{Mu}(T)\lambda_{Mu}(T) + [1 - f_{Mu}(T)]\lambda_D \\ &\simeq f_{Mu}(T)\lambda_{Mu}(0) + \lambda_D,\end{aligned} \tag{6}$$

and we verified this procedure for CdS by comparing this analysis method with the two-component fits of Eq. (4): both methods yield the same ionization energies within experimental errors.

A. CdS

Muon spin rotation asymmetry and the corresponding frequency spectra at a temperature of 5 K of the virgin CdS wafer in the bulk and at $\langle z \rangle \sim 140$ nm are shown in Figs. 2(a)–2(d). In the bulk, a clear beating is visible reflecting the presence of four shallow Mu satellite lines and the center μ^+ line of muons, which do not form shallow Mu. The two lines with smaller splitting and higher intensity are due to shallow Mu at the bonds under 109.4° with respect to the ⟨0001⟩ axis, and the two lines with larger splitting are from shallow Mu at the bond parallel to the ⟨0001⟩ axis. In contrast to the bulk measurements the LEM data do not show any beating which means that in the near-surface region either shallow Mu does not form, or is strongly suppressed, or—due to the presence of defects—fast spin and/or charge exchange with a defect electron causes a "collapse" of the line splitting resulting in a broadening of the diamagnetic line. Recent bulk μSR experiments in CdS and Si demonstrated the reduction of the Mu formation probability in the presence of defects [54]. Rutherford backscattering spectrometry (RBS) channeling measurements with 2-MeV He nuclei at the Institute of Ion Beam Physics at the ETH, Zurich, revealed that a surface layer of at least one μm depth has a high defect concentration, probably caused by the mechanical polishing of the CdS wafer. We attribute the absence of the characteristic shallow Mu lines and the slight broadening of the diamagnetic line in Figs. 2(c) and 2(d) to the presence of these defects. In order to remove the defect-rich surface layer the CdS sample was etched for 55 min at 60° C in a 1:1 HCL/H_2O solution. The final thickness of the wafer was 0.35(4) mm, meaning that a total of ~150 μm of material was removed. After this procedure, the μSR data show the characteristic beating typical for shallow Mu, see Figs. 2(e) and 2(f). Compared to the bulk data the shallow Mu fraction is clearly reduced, and the satellite lines are not resolved due to the shorter time window of 10 μs in LEM. The

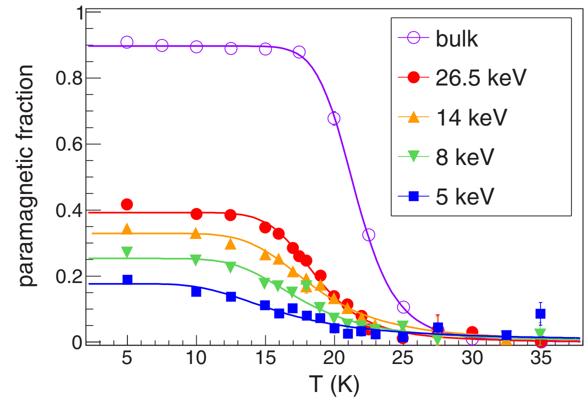

FIG. 3. (Color online) CdS (0001), neutral fraction $f_{Mu}(T)$ as a function of temperature T for different implantation energies. The bulk data are for the virgin sample, and the LE-μSR data are for the etched sample. Solid lines are fits of Eq. (2) to the data to determine the shallow Mu ionization energy.

reduction of the Mu amplitudes even at highest implantation energies is likely to be caused by defects which are still present closer to the surface after the etching procedure.

The neutral fraction $f_{Mu}(T)$ as a function of temperature is shown in Fig. 3, where the μSR asymmetry spectra were fit

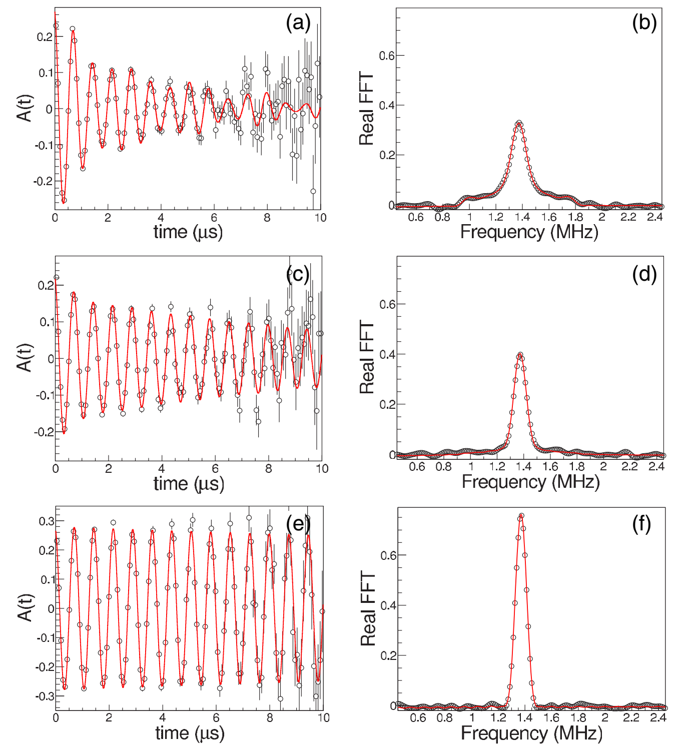

FIG. 4. (Color online) ZnO (0001), 10-mT applied parallel to a ⟨0001⟩ direction, μSR asymmetry spectra $A(t)$, and corresponding real part of fast Fourier transform (Real FFT) of one of the positron counters. (a) and (b) 10 K, implantation energy 17.5 keV ($\langle z \rangle \sim 82$ nm). (c) and (d) 10 K, implantation energy 2.5 keV ($\langle z \rangle \sim 15$ nm). (e) and (f) 60 K, implantation energy 17.5 keV. The solid red lines are fits to the data as described in the text, using the program MUSRFIT [53].

with Eq. (4) to determine the asymmetries $A_D(T)$ and $A_{Mu}(T)$. The decreasing neutral fraction with decreasing implantation energy below 26.5 keV is a characteristic normally observed in insulators and semiconductors [55]. This is attributed to the fact that a substantial fraction of Mu is formed by those thermalized μ^+ which may capture one of the excess electrons generated in its own ionization track (so-called *delayed* Mu formation). The lower the energy the lower the number of track electrons, which reduces the Mu formation probability. Typically, this *delayed* Mu formation saturates if the stopping depth—i.e., the track length—of the μ^+ is of the order of hundred nanometer [55]. This length scale fits to earlier observations where the analysis of μSR experiments with applied electric fields on bulk insulators suggested a similar length scale for *delayed* Mu formation [56]. Bulk μSR experiments on CdS with an applied electric field showed that the recombination of a μ^+ with a track electron is highly suppressed at relatively weak electric fields of about 8 kV/cm [57]. As we will show below, the electric fields due to band bending in CdS at mean implantation depths $\langle z \rangle < 40$ nm (implantation energy <5 keV) are 6–8 kV/cm. This means that the near-surface electric field additionally suppresses Mu formation.

The neutral fraction begins to drop at lower temperature the closer the muons stop to the surface. This reflects the decrease of the Mu ionization energy on approaching the surface and will be discussed in Sec. III C.

B. ZnO

Compared to the CdS data, the shallow Mu lines in ZnO at 10 K are significantly broadened and unresolved, as shown in Figs. 4 and 5. The 10-K data in Figs. 4(a) and 4(c) were fit with five frequencies and fixed splitting of the shallow Mu lines, and the 60-K data in Fig. 4(e)—where shallow Mu is ionized—were fit with a single exponentially relaxing component. The bulk data are very similar to the 17.5 keV data of Fig. 4(a), also revealing unresolved shallow Mu lines. Figure 5 shows the frequency spectra at 10 K as a function of implantation energy, obtained by a maximum entropy fit of the time domain data [51,52]. Similar to the CdS data a clear increase of the diamagnetic line at the expense of the shallow Mu fraction is visible at decreasing implantation energies. We attribute this as well to the decreasing probability for *delayed* Mu formation due to the decreasing number of track electrons, and the presence of an electric field at the surface due to band bending. The higher maximum entropy amplitude of the diamagnetic line at 27 keV compared to 25 keV has its origin in the slightly more narrow line width of the diamagnetic signal at 27 keV (the integral of the line, which equals the asymmetry A_D of the diamagnetic signal, is the same for both energies).

For the determination of the ionization energies at different depths, we use Eq. (5) to fit the μSR asymmetry spectra, and we plot the relaxation rate λ as a function of temperature and implantation energy. This is shown in Fig. 6 for ZnO and the Au/ZnO Schottky barrier. The absolute value of λ is proportional to the Mu fraction $f_{Mu}(T)$ and Eq. (6) has been used to fit the data of Fig. 6. The relaxation rates in Au/ZnO are generally smaller compared to ZnO because of muons stopping in the Au layer which contribute to the diamagnetic signal. Similar to CdS, the relaxation rate, i.e., the neutral fraction, begins to drop at lower temperatures the closer the muons stop at the surface/interface. This is again a manifestation of the decreasing ionization energy.

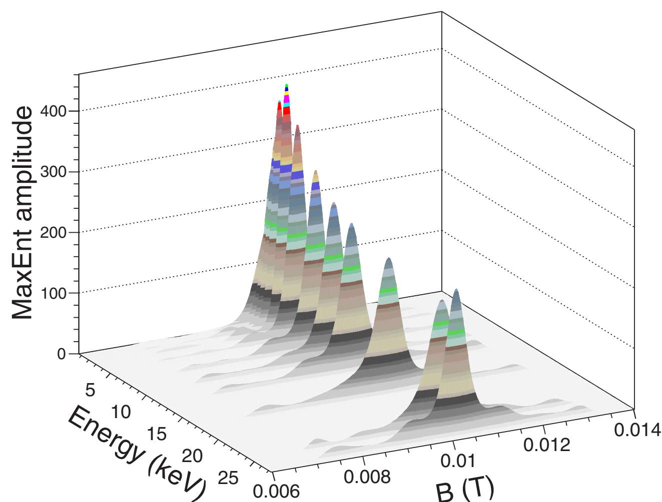

FIG. 5. (Color online) ZnO (0001), 10 K, maximum entropy [51,52] spectra as a function of implantation energy. On lowering, the implantation energy the diamagnetic peak increases at the expense of the shallow Mu satellite peaks.

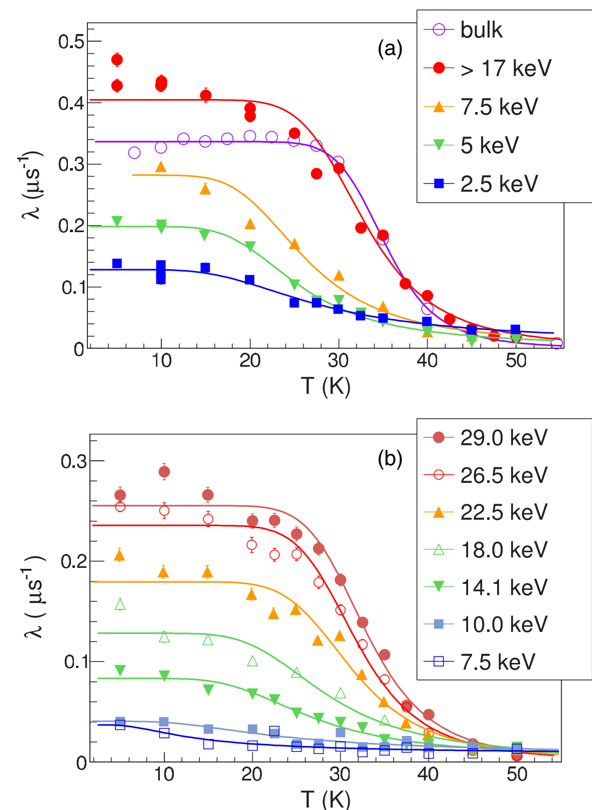

FIG. 6. (Color online) (a) ZnO (0001), single component exponential depolarization rate λ as a function of temperature for different implantation energies. Solid lines are fits of Eq. (6) to the data to determine the shallow Mu ionization energy. (b) 20-nm Au on top of ZnO (0001).

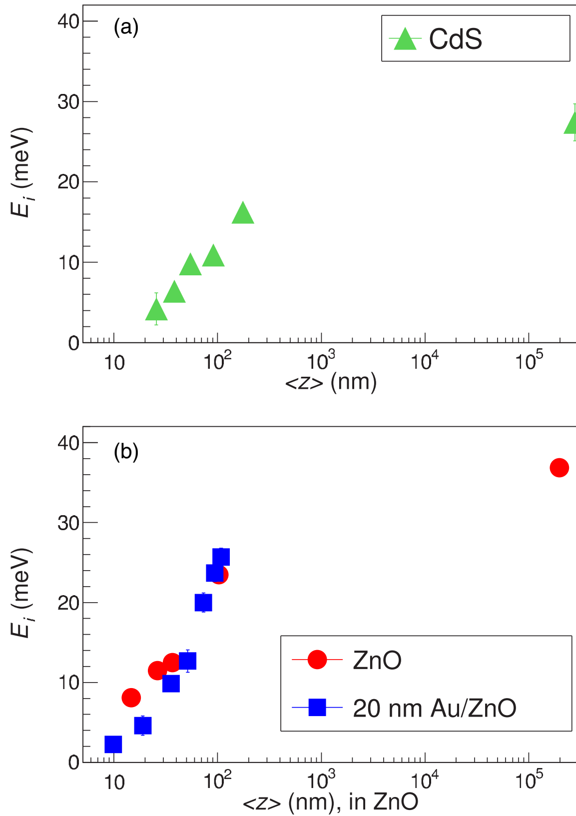

FIG. 7. (Color online) Ionization energy E_i as a function of mean implantation depth $\langle z \rangle$ in (a) CdS and (b) ZnO and Au/ZnO sample. Note that mean depths of $\langle z \rangle > 200$ nm and $\langle z \rangle \lesssim 100$ μm are experimentally not accessible due to the lack of muon beams with energies between 30 keV and ~1 MeV.

C. Depth dependence of the ionization energy of shallow muonium in CdS and ZnO

The depth dependence of the ionization energies in CdS and in ZnO, Au/ZnO, are shown in Fig. 7. Our bulk values ($\langle z \rangle \sim 300$ μm) are in agreement with literature data. At the maximum accessible mean depth in LEM of ~180 nm, the ionization energy is already clearly reduced compared to the bulk value. This reduction is enhanced on approaching the surface, indicating an increase of the internal electric field. In Fig. 7(b), $\langle z \rangle$ denotes the mean depth with respect to the surface in ZnO, and to the metal-semiconductor interface in Au/ZnO. At the Au/ZnO interface the reduction of E_i is larger compared to ZnO on a length scale of about 100 nm. This can be attributed to a larger shift of the ZnO electronic bands at the interface due to the contact to the Au layer, causing a larger band bending, i.e., an enhanced electric field.

The ZnO data suggest a convergence with the bulk ionization energy at a depth of ~0.5 μm, whereas in CdS, this length scale appears to be larger (>1 μm). The room-temperature resistivity of the ZnO wafers is 10 Ωcm, which is hundred times smaller than the resistivity of the CdS wafer. If we assume that this is caused by a hundred times higher free charge carrier concentration n in ZnO, the Debye length $L_D = \sqrt{\varepsilon_r \varepsilon_0 k_B T/(e^2 n)}$ at room temperature, which is a measure of the depth of the band bending region, is expected to be

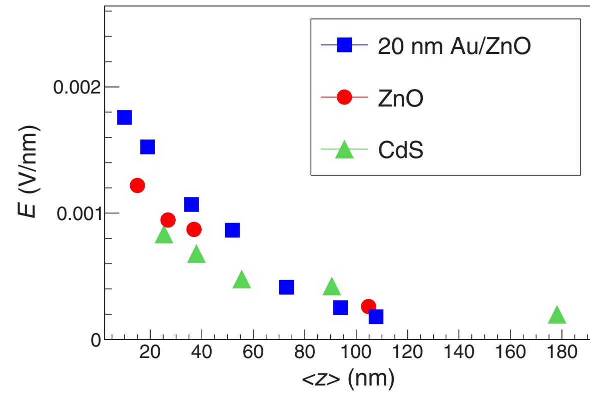

FIG. 8. (Color online) Calculated electric field E as a function of mean depth $\langle z \rangle$ in CdS, ZnO, and Au/ZnO.

about ten times smaller in ZnO. The estimated Debye length of ~0.5 μm in ZnO at ~30 K implies a low temperature charge carrier concentration of $n \sim 5 \times 10^{12}$ cm^{-3}, which is consistent with literature data [58]. The low temperature charge carrier concentration in CdS is then expected to be in the 10^{10} cm^{-3} range to obtain a Debye length of the order of μm.

Using the data of Fig. 7 and the simple one-dimensional model described in Appendix, the electric field as a function of $\langle z \rangle$ can be calculated and is shown in Fig. 8. For ZnO and Au/ZnO data $\langle z \rangle$ means again the distance to the surface (ZnO), or to the Au/ZnO interface. The increase of the electric field close to the Au/ZnO interface due to enhanced band bending is clearly visible. As described in Sec. I a linear increase of the electric field toward the surface/interface is expected. However, the data indicate a deviation from linear dependence, with a faster increase of the field the closer the muons stop to the surface/interface. This could have its origin in the broad stopping distribution of the muons (see Fig. 1): in our simple analysis, we effectively determine an "averaged" ionization energy. The larger the implantation energy the larger the range for the averaging, which may cause the observed deviation from linear dependence.

IV. DISCUSSION

As we noted in Sec. I the binding energy at mean depths $\langle z \rangle > 10$ nm is marginally affected by modifications of the wave function at the semiconductor surface, position dependent effective masses and dielectric constants, and dielectric confinement. The observed changes on E_i in the depth range of our low-energy μSR study (10 nm $< \langle z \rangle <$ 200 nm) can be naturally explained by assuming the presence of an electric field due to band bending. It is then the Poole-Frenkel effect which causes the reduction of E_i, and this allows us to relate the depth-dependent E_i to the electric field profile.

Our results represent the first depth profiling of the ionization energy of a solitary hydrogenlike impurity state over a range of about 200 nm by means of a *local probe* technique. In this context, *local probe* means that the probe resides at an interstitial or substitutional side *within* the sample, where it "observes" its local environment on a nanometer scale, such as e.g., μSR, NMR, β-NMR, ESR, PAC, or Moessbauer spectroscopy. The determination of the depth profile of E_i

at semiconductor surfaces or interfaces by low-energy μSR requires the detectability of the corresponding muonium states, e.g., semiconductors with doping levels $\lesssim 10^{17}$ cm^{-3}, and not too high defect concentration. In Sec. III A, we showed that a significant fraction of Mu in semiconductors is due to *delayed* capture of an electron from the muon's ionization track, where electrons from the track up to distances of 50–100 nm can be captured. Assuming that the muon electron capture probability is reduced in the presence of defects—because defects in semiconductors usually act as recombination centers for excess carriers [59]—a rough estimate for the tolerable defect concentration is given by the requirement that there are no defects in a volume of $\sim$(50 nm)^3 surrounding the stopped muon. This means that the defect concentration should not exceed $\sim 10^{16}$ cm^{-3}.

The determination of the electric-field profile from the depth-dependent change in ionization energy is an indirect method, but it has the advantage that the sample can be studied as it is. This is different to a "surface technique" such as Kelvin probe microscopy (KPM), which can directly measure the potential profile at the surface of cleaved samples. It has been frequently used in semiconductor studies on *pn* junctions, heterostructures, transistors, and solar cells [60], with a spatial resolution in the nanometer range. Unlike μSR, it cannot provide information about the ionization energy of single impurities.

The presented procedure offers the interesting possibility to study the characteristics of shallow impurities in the presence of other dopants: the implantation of solitary impurities allows to indirectly sense the intrinsic charge carrier concentration due its effect on the band bending close to the surface or an interface. The direction of band bending is not accessible here because the changes on the ionization energy only depend on the absolute value of the electric field. Since muon spin rotation is contactless and does not need the application of an electric potential at the surface it provides direct information about intrinsic properties of the semiconductor.

The simplification of the one-dimensional model is well justified if we assume that the minimum of the ionization potential in one direction is the dominant effect on the measured change of the ionization energy. The full three-dimensional (3D) case is discussed by Martin and co-workers for deep impurity levels [18], where the authors calculate the electron emission rate from the impurity state in the 3D case. For example, the electron emission rate is diminshed in positive z direction in the situation sketched in Fig. 9. On the other hand, the electron emission rate is increased by phonon-assisted tunneling and pure quantum mechanical tunneling. For deep levels, pure tunneling becomes important only at very high fields ($\sim 10^7$ V/cm), and a significant emission rate enhancement occurs only for fields $\gg 10^4$ V/cm [18], which are much larger than the electric fields in our experiment.

V. CONCLUSIONS

In summary, we have shown by means of low-energy μSR that the ionization energy of single shallow hydrogenlike muonium states in CdS, ZnO, and Au/ZnO decreases on approaching the semiconductor surface or interface. Compared to the value measured deep in the bulk at $\langle z\rangle \sim 300$ μm the ionization energy is diminshed by $\sim$10 meV at mean depths of 100–150 nm, and further reduced by up to 25–30 meV at a depth of 10 nm. This reduction is attributed to the presence of electric fields (Poole-Frenkel effect) near the surface/interface due to band bending. Other mechanisms potentially able to cause a change of the ionization energy (modifications of the wave function, position dependent effective masses and dielectric constants, dielectric confinement) can be excluded in the investigated depth range. Using a simple one-dimensional model allowed to determine the near-surface/interface electric field profile inside the sample. This kind of investigation recently revealed the presence of a shallow hydrogen donor state in $SrTiO_3$ with decreasing ionization energy at the surface [61]. It can be extended to semiconductors or semiconductor heterostructures with not too high doping levels ($\lesssim 10^{17}$ cm^{-3}) and defect concentrations ($\lesssim 10^{16}$ cm^{-3}).

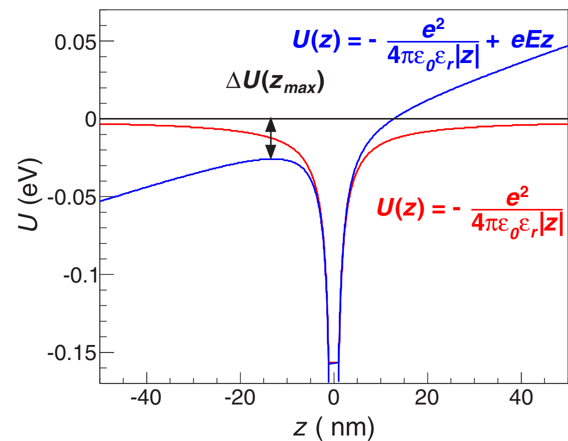

FIG. 9. (Color online) Electric potential energy $U(z)$ as a function of z for a pointlike charge with and without electric field E. For the calculation, we used the relative permittivitiy of $\varepsilon_r = 8.5$ for ZnO and $E = 10$ kV/cm $= 0.001$ V/nm. The double-arrow indicates the position of the local maximum $z_{\rm max}$ of $U(z)$ in the presence of an electric field and the reduction $\Delta U(z_{\rm max})$ of the ionization energy.

ACKNOWLEDGMENTS

We gratefully acknowledge the technical support of H. P. Weber, and the contributions of D. G. Eshchenko in the setup of the LEM facility. We thank J. M. Campos Gil, H. V. Alberto, and R. C. Vilão for stimulating discussions. The μSR measurements were performed at the Swiss Muon Source SμS, Paul Scherrer Institut, Villigen, Switzerland.

APPENDIX: CALCULATION OF THE ELECTRIC FIELD

For the calculation of the electric field at the surface, we use a one-dimensional approximation since we are only interested in the maximum reduction of the ionization energy in the presence of an electric field. The electric potential energy U of a point charge e in the presence of an electric field E along the direction z can be written as

$$U(z) = -\frac{e^2}{4\pi\varepsilon_0\varepsilon_r|z|} + eEz, \tag{A1}$$

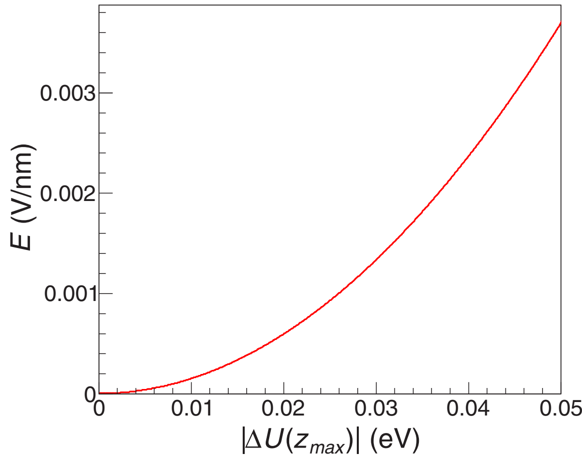

FIG. 10. (Color online) Electric field E as a function of $\Delta U(z_{\max})$, according to Eq. (A3), using the relative permittivity of ZnO, $\varepsilon_r = 8.5$.

where ε_0 is the vacuum permittivity, and ε_r is the relative permittivity of the semiconductor. The change in ionization energy E_i is given by $\Delta U(z_{\max})$, as indicated in Fig. 9. It can be easily derived from Eq. (A1) [16]:

$$\Delta U(z_{\max}) = -e\sqrt{\frac{eE}{\pi\varepsilon_0\varepsilon_r}}. \tag{A2}$$

Solving Eq. (A2) for E, we can write the electric field as a function of the reduction of ionization energy $\Delta U(z_{\max})$ (see Fig. 10):

$$E\,(\Delta U(z_{\max})) = \frac{\pi\varepsilon_0\varepsilon_r[\Delta U(z_{\max})]^2}{e^3}. \tag{A3}$$

We calculated the electric fields shown in Fig. 8 with Eq. (A3), where we used $\Delta U(z_{\max}) = E_i(z > 200\ \mu\text{m}) - E_i(z)$, and $\varepsilon_r = 8.9$ for CdS and $\varepsilon_r = 8.5$ for ZnO.

[1] P. M. Koenraad and M. E. Flatté, Nat. Mater. **10**, 91 (2011).
[2] H. Sellier, G. P. Lansbergen, J. Caro, S. Rogge, N. Collaert, I. Ferain, M. Jurczak, and S. Biesemans, Phys. Rev. Lett. **97**, 206805 (2006).
[3] S. Perraud, K. Kanisawa, Z.-Z. Wang, and T. Fujisawa, Phys. Rev. Lett. **100**, 056806 (2008).
[4] K. Teichmann, M. Wenderoth, S. Loth, R. G. Ulbrich, J. K. Garleff, A. P. Wijnheijmer, and P. M. Koenraad, Phys. Rev. Lett. **101**, 076103 (2008).
[5] A. P. Wijnheijmer, J. K. Garleff, K. Teichmann, M. Wenderoth, S. Loth, R. G. Ulbrich, P. A. Maksym, M. Roy, and P. M. Koenraad, Phys. Rev. Lett. **102**, 166101 (2009).
[6] G. Bastard, *Wave Mechanics Applied to Semiconductor Heterostructures* (Editions de Physique, Les Ulis, 1988).
[7] C. Mailhiot, Y.-C. Chang, and T. C. McGill, Phys. Rev. B **26**, 4449 (1982).
[8] J. D. Levine, Phys. Rev. **140**, A586 (1965).
[9] T.-F. Jiang and Y. Shan, J. Phys. C **18**, 3399 (1985).
[10] M. Diarra, Y.-M. Niquet, C. Delerue, and G. Allan, Phys. Rev. B **75**, 045301 (2007).
[11] A. J. Peter, Int. J. Mod. Phys. B **23**, 5109 (2009).
[12] J. Zak and W. Zawadzki, Phys. Rev. **145**, 536 (1966).
[13] J. M. Luttinger and W. Kohn, Phys. Rev. **97**, 869 (1955).
[14] W. Kohn, in *Solid State Physics*, edited by Frederick Seitz and David Turnbull (Academic Press, New York, 1957), Vol. 5, pp. 257–320.
[15] S. M. Sze and K. K. Ng, *Physics of Semiconductor Devices*, 3rd ed. (John Wiley & Sons, Inc., Hoboken, NJ, USA, 2006).
[16] J. Frenkel, Phys. Rev. **54**, 647 (1938).
[17] J. L. Hartke, J. Appl. Phys. **39**, 4871 (1967).
[18] P. A. Martin, B. G. Streetman, and K. Hess, J. Appl. Phys. **52**, 7409 (1981).
[19] B. D. Patterson, Rev. Mod. Phys. **60**, 69 (1988).
[20] K. H. Chow, B. Hitti, and R. F. Kiefl, in *Semiconductors and Semimetals*, Vol. 51A, edited by M. Stavola (Academic Press, San Diego and London, 1998).
[21] S. F. J. Cox, J. Phys.: Condens. Matter **15**, 1727 (2003).
[22] S. F. J. Cox, Rep. Prog. Phys. **72**, 116501 (2009).
[23] A. Yaouanc and P. Dalmas de Réotier, *Muon Spin Rotation, Relaxation, and Resonance: Applications to Condensed Matter* (Oxford University Press, Oxford, UK, 2011).
[24] C. Kilic and A. Zunger, Appl. Phys. Lett. **81**, 73 (2002).
[25] C. G. Van de Walle and J. Neugebauer, Nature (London) **423**, 626 (2003).
[26] C. G. Van de Walle, Phys. Rev. Lett. **85**, 1012 (2000).
[27] S. F. J. Cox, E. A. Davis, S. P. Cottrell, P. J. C. King, J. S. Lord, J. M. Gil, H. V. Alberto, R. C. Vilão, J. Piroto Duarte, N. Ayres de Campos, A. Weidinger, R. L. Lichti, and S. J. C. Irvine, Phys. Rev. Lett. **86**, 2601 (2001).
[28] E. A. Davis, S. F. J. Cox, R. L. Lichti, and C. G. Van de Walle, Appl. Phys. Lett. **82**, 592 (2003).
[29] D. M. Hofmann, A. Hofstaetter, F. Leiter, H. Zhou, F. Henecker, B. K. Meyer, S. B. Orlinskii, J. Schmidt, and P. G. Baranov, Phys. Rev. Lett. **88**, 045504 (2002).
[30] M. D. McCluskey, S. J. Jokela, K. K. Zhuravlev, P. J. Simpson, and K. G. Lynn, Appl. Phys. Lett. **81**, 3807 (2002).
[31] E. V. Lavrov, J. Weber, F. Börrnert, C. G. Van de Walle, and R. Helbig, Phys. Rev. B **66**, 165205 (2002).
[32] J. M. Gil, H. V. Alberto, R. C. Vilão, J. Piroto Duarte, P. J. Mendes, L. P. Ferreira, N. Ayres de Campos, A. Weidinger, J. Krauser, Ch. Niedermayer, and S. F. J. Cox, Phys. Rev. Lett. **83**, 5294 (1999).
[33] J. M. Gil, H. V. Alberto, R. C. Vilão, J. Piroto Duarte, N. Ayres de Campos, A. Weidinger, J. Krauser, E. A. Davis, S. P. Cottrell, and S. F. J. Cox, Phys. Rev. B **64**, 075205 (2001).
[34] K. Shimomura, R. Kadono, K. Ohishi, M. Mizuta, M. Saito, K. H. Chow, B. Hitti, and R. L. Lichti, Phys. Rev. Lett. **92**, 135505 (2004).
[35] C. G. Van de Walle, Physica B: Condens. Matter **376-377**, 1 (2006).
[36] R. L. Lichti, K. H. Chow, and S. F. J. Cox, Phys. Rev. Lett. **101**, 136403 (2008).
[37] W. Eckstein, *Computer Simulation of Ion-Solid Interactions* (Springer, Berlin, Heidelberg, New York, 1991).

[38] E. Morenzoni, H. Glückler, T. Prokscha, R. Khasanov, H. Luetkens, M. Birke, E. M. Forgan, Ch. Niedermayer, and M. Pleines, Nucl. Instrum. Methods Phys. Res., Sect. B **192**, 254 (2002).

[39] E. Morenzoni, H. Glückler, T. Prokscha, H. P. Weber, E. M. Forgan, T. J. Jackson, H. Luetkens, Ch. Niedermayer, M. Pleines, M. Birke, A. Hofer, J. Litterst, T. Riseman, and G. Schatz, Physica B: Condens. Matter **289-290**, 653 (2000).

[40] T. Prokscha, E. Morenzoni, K. Deiters, F. Foroughi, D. George, R. Kobler, A. Suter, and V. Vrankovic, Nucl. Instrum. Methods Phys. Res., Sect. A **595**, 317 (2008).

[41] D. R. Harshman, A. P. Mills, J. L. Beveridge, K. R. Kendall, G. D. Morris, M. Senba, J. B. Warren, A. S. Rupaal, and J. H. Turner, Phys. Rev. B **36**, 8850 (1987).

[42] E. Morenzoni, F. Kottmann, D. Maden, B. Matthias, M. Meyberg, Th. Prokscha, Th. Wutzke, and U. Zimmermann, Phys. Rev. Lett. **72**, 2793 (1994).

[43] T. Prokscha, E. Morenzoni, C. David, A. Hofer, H. Glückler, and L. Scandella, Appl. Surface Sci. **172**, 235 (2001).

[44] E. Morenzoni, T. Prokscha, A. Suter, H. Luetkens, and R. Khasanov, J. Phys.: Condens. Matter **16**, S4583 (2004).

[45] K. Seeger, *Semiconductor Physics: An Introduction*, 9th ed. (Springer, Berlin, Heidelberg, New York, 2004).

[46] S. F. J. Cox, J. L. Gavartin, J. S. Lord, S. P. Cottrell, J. M. Gil, H. V. Alberto, J. Piroto Duarte, R. C. Vilão, N. Ayres de Campos, D. J. Keeble, E. A. Davis, M. Charlton, and D. P. van der Werf, J. Phys.: Condens. Matter **18**, 1079 (2006).

[47] M. Senba, J. Phys. B **38**, 1305 (2005).

[48] J. M. Gil, J. Piroto Duarte, R. C. Vilão, H. V. Alberto, N. Ayres de Campos, and S. F. J. Cox, Physica B: Condens. Matter **404**, 834 (2009).

[49] R. C. Vilão, A. G. Marinopoulos, R. B. L. Vieira, A. Weidinger, H. V. Alberto, J. Piroto Duarte, J. M. Gil, J. S. Lord, and S. F. J. Cox, Phys. Rev. B **84**, 045201 (2011).

[50] R. Abela, A. Amato, C. Baines, X. Donath, R. Erne, D. C. George, D. Herlach, G. Irminger, I. D. Reid, D. Renker, G. Solt, D. Suhi, M. Werner, and U. Zimmermann, Hyperfine Interact. **120-121**, 575 (1999).

[51] T. M. Riseman and E. M. Forgan, Physica B: Condens. Matter **326**, 226 (2003).

[52] T. M. Riseman and E. M. Forgan, Physica B: Condens. Matter **326**, 230 (2003).

[53] A. Suter and B. Wojek, Physics Procedia **30**, 69 (2012).

[54] H. V. Alberto, R. C. Vilão, J. Piroto Duarte, J. M. Gil, A. Weidinger, J. S. Lord, and S. J. F. Cox, Phys. Rev. B **86**, 035203 (2012).

[55] T. Prokscha, E. Morenzoni, D. G. Eshchenko, N. Garifianov, H. Glückler, R. Khasanov, H. Luetkens, and A. Suter, Phys. Rev. Lett. **98**, 227401 (2007).

[56] D. G. Eshchenko, V. G. Storchak, J. H. Brewer, G. D. Morris, S. P. Cottrell, and S. F. J. Cox, Phys. Rev. B **66**, 035105 (2002).

[57] D. G. Eshchenko, V. G. Storchak, S. P. Cottrell, and S. F. J. Cox, Phys. Rev. B **68**, 073201 (2003).

[58] A. Y. Polyakov, N. B. Smirnov, A. V. Govorkov, E. A. Kozhukhova, S. J. Pearton, D. P. Norton, A. Osinsky, and Amir Dabiran, J. Electron. Mater. **35**, 663 (2006).

[59] D. K. Schroder, *Semiconductor Material and Device Characterization*, 3rd ed. (Wiley, Hoboken, NJ, USA, 2006).

[60] W. Melitz, J. Shen, A. C. Kummel, and S. Lee, Surface Sci. Rep. **66**, 1 (2011).

[61] Z. Salman, T. Prokscha, A. Amato, E. Morenzoni, R. Scheuermann, K. Sedlak, and A. Suter, Phys. Rev. Lett. **113**, 156801 (2014).